PERGAMON

Chemical Engineering Science 58 (2003) 2479–2490

Chemical Engineering Science

www.elsevier.com/locate/ces

Polymerisation of methyl methacrylate in a pilot-scale tubular reactor: modelling and experimental studies

S. Fan[a], S. P. Gretton-Watson[a], J. H. G. Steinke[b], E. Alpay[a,*]

[a] *Department of Chemical Engineering and Chemical Technology, Imperial College London, London, SW7 2AZ, UK*
[b] *Department of Chemistry, Imperial College London, London, SW7 2AZ, UK*

Received 4 December 2002; received in revised form 21 February 2003; accepted 24 February 2003

Abstract

A pilot-scale tubular reactor fitted with in-line static mixers is experimentally and theoretically evaluated for the polymerisation of methyl methacrylate (MMA). A non-isothermal and non-adiabatic axially dispersed plug-flow model is used to describe the flow characteristics of the reactor. The model is applied to the polymerisation of a concentrated MMA solution (up to 72% (v/v)). Key model parameters were attained through independent bench and pilot-scale experiments. Measured monomer conversions and polymer molecular weight were accurately predicted by model simulation. The presence of static mixers is shown to give near-ideal plug-flow operation for the experimental conditions of this study. Furthermore, an approximately four-fold increase in overall heat transfer coefficient is indicated due to the radial mixing incited by the mixers. Studies also demonstrated the importance of inhibitor kinetics on the dynamic and steady-state performance of the reactor.

Keywords: Polymerisation; Tubular reactor; Static mixer; Heat transfer; Modelling

1. Introduction

Polymerisation processes can be highly exothermic and often exhibit non-linear thermophysical properties. This leads to potential problems in the control of end-user properties, which are strongly influenced by the local operating conditions and the properties of the reaction medium, as well as any spatial or temporal variations of these in the reactor. Economic and competitive pressures often necessitate polymer producers to develop new products and/or employ processing technologies which are adept for high-throughput and consistent product quality. Although most polymers are produced under batch processes, the few that are made continuously dominate industrial output (Nauman, 1994). In recent times, tubular reactor operations have become increasingly attractive as a means of controlling both the residence time distribution of the active polymer molecules and the reaction temperature (Hamer & Ray, 1986a,b; Fleury, Meyer, & Renken, 1992; Zacca & Ray, 1993; Melo, Biscaia, & Pinto, 2001a). However, conventional tubular reactor operation is often unfeasible due to the high viscosity of the reaction medium, and subsequently an impractical (and even impossible) means of achieving the flow velocities necessary for the plug flow of the reactants, and for adequate heat transfer between the reaction medium and tube walls. Tubular systems employing axial rotors and, more recently, in-line static mixers, are possible means of achieving the radial mixing characteristic of plug-flow operation, with subsequent benefits of enhanced heat transfer between the bulk fluid and the tube-wall region. The simplicity of the static mixer designs, as well as their pliability for either single-pass and loop-reactor operations (see Section 2), makes this technology particularly attractive. A full-scale polystyrene process has been jointly developed in Japan by Sulzer Brothers, Dainippon Ink & Chemicals, and Sumitomo Heavy Industries with a similar configuration. Nevertheless, very few studies have considered the detailed characterisation and modelling of such units under conditions of polymerisation. Similarly, the dynamic response of static-mixer-based reactors is unknown, but would provide valuable information on reactor controllability, and on operating modes which involve user-specified transitions from one product specification to another. However, studies to date have principally focussed on steady-state operation (e.g. Baillagou & Soong, 1985a,b; Fleury et al., 1992).

As discussed by Fleury et al. (1992), static mixers provide an effective means of radial mixing for very low

* Corresponding author.
E-mail address: e.alpay@imperial.ac.uk (E. Alpay).

0009-2509/03/$ - see front matter © 2003 Elsevier Science Ltd. All rights reserved.
doi:10.1016/S0009-2509(03)00119-2

Reynolds numbers, and thus a possible approach to the ideal plug-flow situation for highly viscous media. The authors subsequently used an ideal plug-flow assumption in modelling a pilot-scale loop (recycle) reactor equipped with static mixers. Specific attention was given to methyl methacrylate (MMA) solution polymerisations at relatively high operating temperatures, i.e. temperatures considerably above the glass transition of PMMA. Due to the high recycle ratio employed in the experimental studies, the continuous well-mixed flow condition was approached, which was subsequently supported by simulation results. However, for industrial scale production using, for example, relatively large diameter tubular sections, and operating under conditions close to the glass transition, ideal plug flow is unlikely to be achieved, and a more rigorous theoretical evaluation is anticipated; see also the discussions of Melo et al. (2001b). For example, in earlier work by Baillagou and Soong (1985c), a rheokinetic model for MMA polymerisation in a tubular reactor was found to give marked improvements in predictions when compared to the ideal plug-flow situation (but nevertheless over-estimated measured conversion data). These studies considered a reactor arrangement in which static mixers were employed towards the end of a 5 m reactor tube, i.e. in a 1.5 m region where viscosity and heat transfer issues were deemed to be of particular significance. The rheokinetic model specifically accounted for the velocity profile of the reaction medium, axial and radial diffusion, and conversion-dependent kinetics in the region of the gel (Trommsdorff) effect. Nevertheless, it was not clear from this study as to whether velocity-profile distribution was of explicit importance in the static mixer section of the reactor.

In this work, theoretical and experimental studies of a pilot-scale reactor system employing in-line static mixers are presented. Particular attention is given to the transient response of the reactor during start-up, and to changes in operating temperature during the course of reaction. The dynamic studies provide an acute test on model reliability in terms of mixing phenomena and heat transfer characteristics, and thus a rigorous means of evaluating any deviations from the near-ideal plug-flow situation. As a case study, the polymerisation of MMA has also been considered in this work; such a well-characterised reaction enables focus on reactor hydrodynamics and kinematics, and specifically the nature and efficacy of mixing associated with the static mixers. Attention is given to the prediction of both transient conversion and average molecular weight trends. Studies are conducted for different space–times for a single-pass reactor configuration, which depicts a conventional tubular reactor arrangement.

2. Experimental

The pilot-plant polymerisation reactor is shown schematically in Fig. 1. The reactor has the flexibility of being able to operate under a number of modes such as loop or single-pass. The mode of operation performed in the following polymerisation experiments was single-pass. This can be achieved by having the gear pump inactive during the experiment. As a result this section of the reactor was blocked and hence allows single-pass mode to occur. The reactor tubes have an inside diameter of 32 mm and a total length of 5.4 m. The interior of the tubes is fitted with SMXL static mixers (supplied by Sulzer Chemtech Ltd) and is entirely made from 316 stainless steel. The reactor tubes are jacketed; three independent heat exchangers control the temperature of three sections of the reactor, i.e. the loop, tubular, and devolatilisation sections in the arrangement shown in Fig. 1. The reactor pressure can be controlled using a pressure control valve, which is situated prior to the devolatilisation section. The reactor additionally has three sampling points, three micro-dosing pumps and an on-line data acquisition system. HP VEE version 5.01 was used to monitor and save the reactor temperatures and pressures every 30 s in a PC. The sampling points are located along the single-pass tubular reactor at lengths 0.89, 3.37 and 4.48 m.

The following reagents were used in the experiments: MMA (99%, supplied by Lancaster Ltd., UK), xylene (99%, supplied by Fisher Scientific UK), AIBN (2,2′azobisisobutyronitrile, 97%, supplied by Fisher Scientific UK), 2,6-di-tert-butyl-4-methylphenol (99%, supplied by Lancaster Ltd., UK), dichloromethane (99% GPR, supplied by BDH), and hexane (95%, supplied by BDH). The MMA was stabilised with 60–100 ppm 4-methoxyphenol as inhibitor. All the materials were used without further purification, which conforms with typical industrial practise.

In the following sections, experimental details are given for three general types of experiments carried out. The first was to establish the temperature dynamics of the reactor system in the absence of reaction (the so-called “cold run”), and thus basic validation of the heat transfer model. Bench-scale polymerisation experiments were also performed to validate reaction kinetics, and to establish certain key parameters (see Section 4.2). Having established heat transfer and reaction kinetic issues, pilot-scale polymerisation studies were then carried out.

2.1. Temperature dynamics of the pilot-plant reactor

Prior to the reaction studies, it was important to determine the heat transfer characteristics of the reactor. Experiments were thus carried out to measure the transient and steady-state temperature profiles of the reactor for jacket temperature step changes. Such experiments were conducted with the reactor initially full of xylene and at a steady-state temperature of 20°C. In the first experiment (cold run #1), jacket temperature step changes to 70°C and then 100°C were carried out. During these experiments, fresh xylene at a temperature of 20°C was continuously fed to the reactor. In cold run #2, similar dynamic experiments were carried

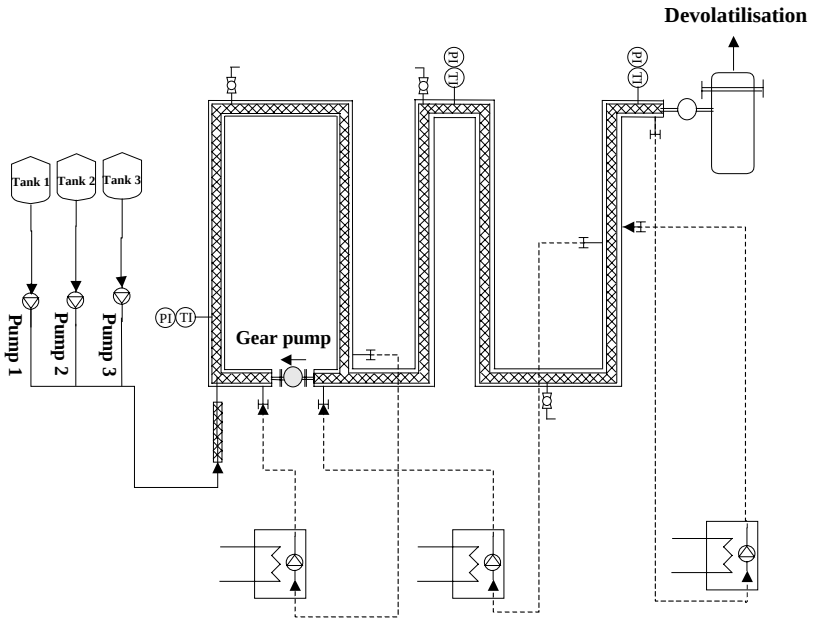

Fig. 1. The pilot-plant reactor system.

Table 1
Temperature step testing experiments

Experiment	$F_f(\times 10^{-6})$	$F_r(\times 10^{-6})$	T_{jsp}-0	T_{jsp}-1	T_{jsp}-2	τ_j	U_0 (exp)	U_0 (model)
Cold run # 1	0.15	42.45	20	70	100	84	0.22	0.22
Cold run # 2	0	16.53	20	38	—	42	0.16	0.16
PMMA # 4	0.84	0	20	70	—	—	0.06	0.059

out, but there was no inflow of xylene and the recycle flow rate was different. For both cold run #1 and #2 the recycle pump was in operation, therefore the reactor was operating in a loop mode followed by a single-pass section. Other experimental conditions for the two experiments are summarised in Table 1. The two sets of independent experiments allowed the reactor parameter estimation of the overall heat transfer coefficient (under conditions of no polymer) and the jacket temperature time constant, under very different operating conditions; see Section 4.1.

2.2. Bench-scale polymerisation studies

It was necessary to validate the kinetic model structure and parameters used within the simulation, and specifically to examine the inhibition effects caused by the inhibitor with which MMA is stabilised. This was achieved by performing a number of bench-scale (batch) experiments. These were carried out in a 250 ml three-necked round bottom flask fitted with condenser and nitrogen supply. Agitation was achieved using a mechanical stirrer (Janke & Kunkel RW20 DZM).

The reaction vessel was charged with xylene (0.59 mol, 79 ml) and MMA (0.30 mol, 32 ml) at room temperature. AIBN (1.80 mmol, 300 mg) was added and once dissolved the resulting solution cooled with a liquid nitrogen bath for 5 min. An atmosphere of nitrogen was introduced by passing a stream of nitrogen through the solution. After 30 min the solution was cooled until frozen with a liquid nitrogen bath. Degassing with nitrogen recommenced for 5 min once the solid had thawed. The freeze-thaw cycle was repeated twice, before the flask was introduced into a thermostatically controlled water bath preheated to 80°C (±0.1°C). Agitation of the solution was then initiated (515 rpm). The reaction temperature was kept constant throughout the polymerisation process lasting 7 h. Aliquots were taken from the reaction mixture every 20 min via an airtight PTFE-lined syringe. Approximately 2 ml of sample solution was taken and mixed with a pre-weighed ambient temperature solution of xylene (2 ml) and 2,6-di-tert-butyl-4-methylphenol (1.80 mmol, 397 mg). The sample vial was then re-weighed, placed into a liquid nitrogen bath for 40–50 s and stored at 4°C for precipitation. Upon completion of the polymerisation, the remaining solution was diluted with an equal volume of a 0.90 molar solution of 2,6-di-tert-butyl-4-methylphenol in xylene, placed in a liquid nitrogen bath for 5 min and finally stored at 4°C.

Table 2
MMA polymerisation operation conditions

Operation parameter	PMMA #3	PMMA #4	Unit
Pressure	8.0	8.0	bar
F_f	1.11×10^{-6}	0.842×10^{-6}	m^3/s
T_f	20	20	°C
T_{jsp}	70 − 80	70	°C
C_{mf}	2.15	6.52	$kmol/m^3$
C_{if}	0.0788	0.0413	$kmol/m^3$
C_{zf}/C_{mf}	1.0×10^{-4}	1.0×10^{-4}	—
r_{ec}	0	0	—

Precipitation of the polymer was achieved through the drop-wise addition of the stored polymer solutions to a stirred solution of 10 times its volume of methanol. The precipitate was filtered (Whatman, Grade 1) and finally dried in a vacuum oven at 50°C until constant weight. From the weight of the dry polymer the conversion was determined gravimetrically based on the initial concentration of the polymerisation mixture (see Fig. 4).

2.3. Pilot-scale polymerisation studies

Operating conditions used in the polymerisation experiments (PMMA #3 and PMMA #4) are summarised in Table 2. Before fed to the reactor, AIBN/xylene solution and MMA were degassed separately by purging the liquids with Argon for 12 h. The degassed solutions were then transferred to the reactor feed tanks under an Argon atmosphere. As mentioned above, the reactor configuration used in each experiment was the single-pass mode. Initially, the reactor contained pure xylene at a temperature of 70°C, thus depicting a typical start-up situation. The reaction was initiated by the continuous flow of MMA, xylene and AIBN into the reactor, which was considered as time zero of the polymerisation experiment. The flow rate from each pump was set to achieve the desired reactant concentration. For run PMMA #3, the polymerisation reaction was carried out for 4 h with the jacket temperature maintained at around 70°C for 2 h, and then changed to 80°C. Whereas, for run PMMA #4, the reaction was conducted over 3 h with the jacket temperature maintained at 70°C (see Table 2). During the polymerisation, aliquots were taken from the three sample ports along the reactor length every 20 min. Samples were quenched in a solution of cold xylene and inhibitor, and precipitated by adding an excess methanol. Monomer conversion was thus again determined by the direct gravimetric method described in Section 2.2. The molecular weight distribution of each sample was determined in THF at 1 ml/min flow rate at 30°C using a Viscotek 'TriSEC 2000' GPC, TDA 302 detectors and TriSEC Version 3 software for data analysis. The detectors used were refractive index, differential pressure and light scattering.

Table 3
Free radical MMA polymerisation mechanism

Initiation		
	$I \xrightarrow{k_d} 2\dot{I}$	
	$\dot{I} + M \xrightarrow{k_i} P_1$	
Propagation		
	$P_n + M \xrightarrow{k_p} P_{n+1}$	
Termination		
	$P_n + P_m \xrightarrow{k_{tc}} D_{n+m}$	(Combination)
	$P_n + P_m \xrightarrow{k_{td}} D_n + D_m$	(Disproportionation)
Chain transfer		
	$P_n + M \xrightarrow{k_{fm}} D_n + P_1$	(To monomer)
	$P_n + S \xrightarrow{k_{fs}} D_n + P_1$	(To solvent)
Inhibition		
	$f_z P_n + Z \xrightarrow{k_z} D_n$	

3. Mathematical modelling

3.1. Kinetics of MMA polymerisation

The kinetics of MMA polymerisation is described by the usual free radical polymerisation mechanism (see, for example, Baillagou & Soong, 1985b; Pinto & Ray, 1996), key reactions for which are summarised in Table 3. Based on this mechanism, the kinetic model can be described by the following equations:

$$R_m = -(k_p + k_{fm})C_m\xi_0, \tag{1}$$

$$R_i = -k_d C_i, \tag{2}$$

$$R_z = -k_z C_z \xi_0, \tag{3}$$

$$R_{\xi 0} = 2fk_d C_i - k_t\xi_0^2 - f_z k_z C_z \xi_0, \tag{4}$$

$$R_{\xi 1} = 2fk_d C_i + k_p C_m \xi_0 + (k_{fm}C_m + k_{fs}C_s)(\xi_0 - \xi_1) - k_t\xi_0\xi_1, \tag{5}$$

$$R_{\xi 2} = 2fk_d C_i + (2\xi_1 + \xi_0)k_p C_m + (k_{fm}C_m + k_{fs}C_s) \times (\xi_0 - \xi_2) - k_t\xi_0\xi_2, \tag{6}$$

$$R_{\mu 0} = (k_{fm}C_m + k_{fs}C_s)\xi_0 + (k_{td} + 0.5k_{tc})\xi_0^2, \tag{7}$$

$$R_{\mu 1} = (k_{fm}C_m + k_{fs}C_s + k_t\xi_0)\xi_1, \tag{8}$$

$$R_{\mu 2} = (k_{fm}C_m + k_{fs}C_s)\xi_2 + k_t\xi_0\xi_2 + k_{tc}\xi_1^2. \tag{9}$$

In the above equations, subscripts m, i, and z denote the monomer, initiator and inhibitor respectively, and ξ_i and μ_i denote the ith moment of living and dead polymer, respectively. Rate constants of the model are summarised in Table 4.

Table 4
Kinetic rate constants

Parameter	Reference
$k_d = 1.58 \times 10^{15} \exp(-1.2874 \times 10^5/RT)$	Pinto and Ray (1995)
$k_{p0} = 7.0 \times 10^6 \exp(-2.6334 \times 10^4/RT)$	Pinto and Ray (1995)
$k_{t0} = 1.76 \times 10^9 \exp(-1.1704 \times 10^4/RT)$	Pinto and Ray (1995)
$k_{tc} = k_t$	Brandrup et al. (1999)
$k_{td} = 0$	Brandrup et al. (1999)
$k_{fm} = 4.661 \times 10^9 \exp(-7.4479 \times 10^4/RT)$	Baillagou and Soong (1985b)
$k_{fs} = 1.49 \times 10^9 \exp(-6.6197 \times 10^4/RT)$	Brandrup et al. (1999)
$R = 8.314$	Perry and Green (1984)
$f_0 = 0.53$	Brandrup et al. (1999)
$C = 0.06$	Experimental validation
$k_z = 250k_p$	Brandrup et al. (1999) and Experimental validation
$f_z = 3.4$	Experimental validation

Table 5
Gel and glass effect constitutive equations (Baillagou & Soong, 1985a; Soroush & Kravaris, 1992)

$$k_p = k_{p0}/(1 + k_{p0}\xi_0/Dk_{\theta_p})$$
$$k_t = k_{t0}/(1 + k_{t0}\xi_0/Dk_{\theta_t})$$
$$D = \exp\left(\frac{2.303(1-\phi_p)}{0.168 - 8.21 \times 10^{-6}(T-387)^2 + 0.03(1-\phi_p)}\right)$$
$$k_{\theta_p} = 3.0233 \times 10^{13} \exp(-1.1700 \times 10^5/RT)$$
$$k_{\theta_t} = 1.4540 \times 10^{20} C_{if} \exp(-1.4584 \times 10^5/RT)$$

For the termination (k_t) and propagation (k_p) rate constants expressions are given at the initial onset of polymerisation. During the polymerisation process, the viscosity of the reaction mixture will increase with monomer conversion. This hinders the diffusion of polymeric radicals (i.e. gel effect), which subsequently results in the sharp decrease of the termination rate. At very high conversions, the mobility of the monomer is also influenced (i.e. glass effect), resulting in the decrease of the propagation rate. Several semi-empirical relationships have been proposed to quantify the gel and glass effects, e.g. through modification of the termination and propagation rate constants respectively. The equations of Baillagou and Soong (1985a) were adopted in this work (see Table 5), and provide a convenient means of adjusting the rate constants as the polymer fraction increases.

The initiator efficiency, f, appearing in Eqs. (4)–(6) denotes the fraction of initiator free radicals successful in initiating polymerisation. It decreases as the viscosity of the reaction medium increases (Ghosh, Gupta, & Saraf, 1998). For MMA polymerisation this effect can be more prominent than the influence of diffusion on the propagation rate (Tefera, Weickert, & Westerterp, 1997). In this work, the free volume theory is used (Dube, Soares, Penlidis, & Hamielec, 1997) to model this phenomenon

$$f = f_0 \exp(-C(1/V_F - 1/V_{F\mathrm{cr}})), \tag{10}$$

where f_0 is the initial initiator efficiency and C is a parameter which modifies the rate of change of the efficiency. The free volume (V_F) and critical free volume ($V_{F\mathrm{cr}}$) are given by

$$V_F = 0.025 + 0.001(T-167)\phi_m + 0.00048(T-387)\phi_p + 0.00048(T-249)\phi_s, \tag{11}$$

$$V_{F\mathrm{cr}} = 0.1856 - 2.965 \times 10^{-4}(T-273), \tag{12}$$

and where ϕ_m, ϕ_p, and ϕ_s are the volume fraction of monomer, polymer and solvent

$$\phi_m = C_m MW_m/\rho_m, \tag{13}$$

$$\phi_p = \mu_1 MW_m/\rho_p, \tag{14}$$

$$\phi_s = 1 - \phi_m - \phi_s. \tag{15}$$

The kinetic model structure and parameters were independently validated through the bench-scale experiments described above. For the inhibition reaction (Eqs. (3) and (4)), one inhibitor molecule is assumed to terminate f_z free radicals (Pinto & Ray, 1996). The inhibition rate constant, k_z, is typically proportional to the chain propagation constant (Brandrup, Immergut, & Grulke, 1999). These two parameters were also estimated from the bench-scale experiments along with C in Eq. (10).

3.2. Mass and energy balances

With reference to Fig. 2, the pilot plant reactor is schematically described by 4 tubular sections, i.e. a forward loop section (L_1), a recycle loop section (L_2), a straight-flow section (L_3) and the devolatilisation section (L_4). The recycle loop is not considered in this study, except for the simulation of the pure xylene temperature dynamic experiments. Mixing of the monomer, solvent and initiator at the reactor entrance was modelled as an ideal well-mixed system; a well-mixed system (CSTR) was also assumed for the recycle pump when operating in loop mode. By using in-line SMXL mixers, the residence time distribution of a 1-m tubular section has been reported to correspond to approximately 25–30 ideal mixed cells in series (see Sulzer, 1997 and the discussions below). Thus approximately uniform concentration, temperature and velocity distributions are expected over the flow cross-section, i.e. an approach to the plug-flow situation. However, in this work, any deviations from the ideal plug-flow situation were described by an axially dispersed plug-flow model. The mass balance equations for the concentration of monomer, C_m, initiator, C_i, and inhibitor, C_z, the first three moments of living polymer chains, ξ_0, ξ_1, ξ_2, and the first three moments of dead polymer chains, μ_0, μ_1, μ_2 are then given by

$$\frac{\partial C_x}{\partial t} + \frac{\partial(v_z C_x)}{\partial z} = R_x + D_e \frac{\partial^2 C_x}{\partial z^2}, \tag{16}$$

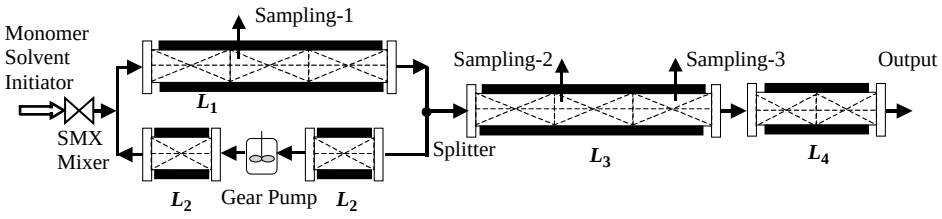

Fig. 2. Schematic equivalent of the loop-tubular reactor.

where C_x denotes the concentration of the above 9 species in each tubular reactor section, L_1 to L_4. The solvent concentration, C_s, can then be calculated from mass continuity (cf. Eq. (15))

$$\frac{C_s MW_s}{\rho_s} + \frac{C_m MW_m}{\rho_m} + \frac{\mu_1 MW_m}{\rho_p} = 1. \tag{17}$$

The energy balance for each reactor section adopts a similar form to that used by Pinto and Ray (1995) and Melo et al. (2001a)

$$(\varepsilon_{\text{mix}}\rho_{\text{mix}}C_p + \varepsilon_r\rho_r C_{p,r})\frac{\partial T}{\partial t} + \rho_{\text{mix}}C_p\frac{\partial(v_z T)}{\partial z} = -R_m(-\Delta H_P) - \frac{4U(T-T_j)}{d_t} + \alpha_t\rho_{\text{mix}}C_p\frac{\partial^2 T}{\partial z^2}. \tag{18}$$

The thermal capacitance of the reaction mixture, tubular walls and static mixers are combined in the above equation. Such an approach assumes thermal equilibrium between the three substrates, which may approximately hold for the thin-bodied static mixers, but cannot be strictly true for the reactor walls. Nevertheless, such an approximation enables some accommodation of the influence of the wall thermal mass on temperature dynamics, without inclusion of a separate dynamic energy balance on the reactor walls. The parameter, ε_r, in Eq. (18) denotes the volume fraction occupied by the static mixers and the reactor walls, and is based on a total volume calculated from the tube outer diameter, d_t. This could be determined from the relationship $\varepsilon_r = 1 - \varepsilon_{\text{mix}}$, where ε_{mix} is the void fraction of the reactor in the presence of static mixers. Note that it has been subsequently shown that temperature profiles are relatively insensitive to the approximation of thermal equilibrium made in the above equation.

The jacket temperature T_j is controlled by a thermostat and is assumed to be uniform in any given section. A well-mixed flow situation is assumed in modelling the jacket dynamics for each reactor jacket section, such that

$$\tau_j\frac{\mathrm{d}T_j}{\mathrm{d}t} + T_j = T_{jsp}, \tag{19}$$

where τ_j is time constant, T_{jsp} is the setpoint of the thermostat. Due to its quick response compared to the mean residence time of reactants in the reactor, a single τ_j was used for all the jacket sections. Its value was determined from the temperature dynamic experiments described in Section 2.1.

As reaction proceeds, the velocity of the reaction mixture, v_z, changes with axial position. By considering the total fluid volume change with reaction, this velocity can be described by (Zacca & Ray, 1993)

$$\frac{\partial v_z}{\partial z} = \frac{R_m MW_m}{\rho_m} + \frac{R_{\mu 1} MW_m}{\rho_p}. \tag{20}$$

The change of reactant densities with temperature can also be easily incorporated into the above velocity equation.

3.3. Auxiliary equations

3.3.1. Physical properties

The density of the reaction mixture of monomer, solvent, polymer and initiator is given by

$$\rho_{\text{mix}} = (\mu_1 + C_m)MW_m + C_s MW_s + C_i MW_i. \tag{21}$$

The specific heat capacity of reaction mixture C_p is calculated from the mole-fraction-average value of components (Perry & Green, 1984)

$$C_p = \frac{\mu_1 C_{p,p} + C_m C_{p,m} + C_s C_{p,s}}{\mu_1 + C_m + C_s}. \tag{22}$$

The viscosity of a polymerisation mixture can increase by several orders of magnitude as reaction proceeds; see also discussions in Section 4.3. Viscosity was not measured on-line in this work. Model predictions of molecular weight were used to infer the viscosity. Note that the viscosity of MMA is similar to that of xylene at 70°C, i.e. $\eta_0 = 0.34 \times 10^{-3}$ Pa s (Perry & Green, 1984). The viscosity of PMMA solution, η, is influenced by the polymer concentration, molecular weight and temperature, such that

$$\eta = \eta_0(1 + \eta_{\text{sp}}), \tag{23}$$

where the specific viscosity η_{sp} is a function of intrinsic viscosity $[\eta]$ and the polymer concentration c, i.e.

$$\eta_{\text{sp}}/c = [\eta](1 + k_h[\eta]c), \tag{24}$$

$$c = \mu_1 MW_m/10^3, \tag{25}$$

and where k_h is the Huggins constant. In this work, the Mark–Houwink–Sakurada equation (Brandrup et al., 1999) was used to determine the intrinsic viscosity of the PMMA solutions

$$[\eta] = 6.75 \times 10^{-3}(M_w)^{0.72}. \tag{26}$$

3.3.2. Effective axial dispersion coefficient

For a parabolic velocity profile in an empty tube, the axial dispersion coefficient D_e can be estimated as (Chen & Nauman, 1989)

$$D_e = D_l + \frac{v_z^2 d_t^2}{192 D_l}. \tag{27}$$

The molecular diffusion coefficient D_l is approximately 10^{-9} m^2/s, and v_z is approximately 1.2×10^{-3} m/s, which yields D_e of an empty tubular reactor with similar configurations to this work as approximately 0.01 m^2/s. In the presence of static mixers, the Bodenstein number, $N_{Bo} = v_z L/D_e$, is reported to typically exceed a value of 50 for one meter length (Sulzer, 1997). This corresponds to at least 26 mixed tanks in series, and thus an approach to the near-ideal plug flow is expected. The effective axial dispersion coefficient D_e can then be estimated from

$$D_e = \frac{v_z L}{N_{Bo}} \sim 2.4 \times 10^{-5} \text{ m}^2/\text{s}. \tag{28}$$

The thermal axial dispersion coefficient α_t in Eq. (18) was set to be 6 times higher than D_e (Nauman, 2001). The influences of these two parameters on reactor performance were analysed through simulation (sensitivity) studies; see Section 4.3.

3.3.3. Heat transfer coefficient

The overall heat transfer coefficient, U, changes with monomer conversion because of the changes in the physical properties of the reaction medium, as well as possible changes in macroscopic mixing patterns. It is therefore important to model U as a distributed parameter along the length of the reactor. For low conversions, the relatively low viscosity of the monomer solution, and its well-characterised properties, enables the use of established heat transfer correlations. Furthermore, it is expected that the tube-side heat transfer film controls the overall rate of heat transfer, such that U at zero conversion (U_0) can be approximated by a conventional tube-side heat transfer coefficient, h_i. For the monomer solution under the experimental conditions of this work, the flow pattern is laminar ($N_{Re} < 100$). A modified form of the Sieder–Tate relationship (Perry & Green, 1984) can thus be used to calculate h_i in the absence of polymerisation

$$\frac{h_i d_t}{\lambda_{\text{mix}}} = 1.86 N_{Gz}^{1/3} \left(\frac{\eta}{\eta_w}\right)^{0.14}, \tag{29}$$

where $N_{Gz} = N_{Re} N_{Pr} d_t/L_e$, $N_{Re} = d_t v_z \rho_{\text{mix}}/\eta$, and $N_{Pr} = \eta C_p/\lambda_{\text{mix}}$ correspond to the Graetz, Reynolds and Prandtl numbers of the reaction mixture. The presence of the static mixer is accounted for by the parameter L_e in the Graetz number, which denotes an "effective length" of the tubular section in the presence of a static mixer. This parameter could be readily determined from the heat transfer studies with a non-reacting medium. The thermal conductivity of the monomer solution, λ_{mix}, appearing in Eq. (29) can be calculated from (Baillagou & Soong, 1985c)

$$\lambda_{\text{mix}} = (\lambda_m \phi_m \rho_m + \lambda_s \phi_s \rho_s + \lambda_p \phi_p \rho_p)/\rho_{\text{mix}}, \tag{30}$$

where in this case, $\phi_p = 0$. For the monomer solution, the viscosity at the reactor wall (η_w) in Eq. (29) can be assumed to be approximately equal to that of bulk (η). This assumption is not expected to hold in the presence of polymer, i.e. at relatively high solution viscosities. Likewise, the complex radial mixing incited by the presence of the static mixers is expected to lead to enhanced heat transfer, and thus an increase in any effective heat transfer coefficient. Furthermore, preliminary trials indicated that in the presence of polymer, Eq. (29) significantly underestimates the overall heat transfer coefficient, even when accounting for the change in the thermal conductivity of the reacting mixture through use of Eq. (30). Thus, to account for the influences of high viscosity, complex mixing, and the effective fluid thermal conductivity on U, a semi-empirical relationship was proposed in this work

$$U = U_0 + \alpha_1 \phi_p + \alpha_2 \phi_p^2 + \alpha_3 \phi_p^3, \tag{31}$$

where ϕ_p is the volume fraction of polymer, and α_1, α_2, and α_3 are model parameters. ϕ_p was considered a key variable for such a relationship in that: (i) an increase in ϕ_p is associated with an increase in viscosity, and thus to potentially greater difference in viscosity between the bulk and wall positions; (ii) the macro-mixing arising from flow-splitting and re-combination around static mixers elements is expected to be more pronounced as $\phi_p$increases; (iii) as polymer content increases, an increase in thermal conductivity is expected.

3.3.4. Molecular weight and conversion

The number and weight average molecular weights and the polydispersity index can be calculated by the method of moments

$$M_n = \frac{\mu_1 + \xi_1}{\mu_0 + \xi_0} MW_m, \tag{32}$$

$$M_w = \frac{\mu_2 + \xi_2}{\mu_1 + \xi_1} MW_m, \tag{33}$$

$$PDI = \frac{M_w}{M_n}. \tag{34}$$

The conversion at any given sampling point is, by definition

$$X_m = \frac{\mu_1}{C_{mf}}. \tag{35}$$

The physical and reactor parameters used in this study are given in Tables 6 and 7, respectively.

3.4. Boundary and initial conditions

The boundary and initial conditions used for the solution of the governing differential equations (16), (18)–(20) can

Table 6
Physical property parameters

Physical parameter	Reference
$\rho_m = 915.1$	Brandrup et al. (1999)
$\rho_s = 886.0$	Perry and Green (1984)
$\rho_p = 1200$	Brandrup et al. (1999)
$\rho_i = 915.0$	Baillagou and Soong (1985a)
$\rho_r = 7830$	Perry and Green (1984)
$MW_m = 100.12$	Brandrup et al. (1999)
$MW_s = 106.17$	Brandrup et al. (1999)
$MW_i = 164.21$	Brandrup et al. (1999)
$-\Delta H_P = 5.78 \times 10^4$	Brandrup et al. (1999)
$C_{p,m} = 1.648$	Baillagou and Soong (1985a)
$C_{p,s} = 1.70$	Brandrup et al. (1999)
$C_{p,p} = 1.47$	Brandrup et al. (1999)
$C_{p,r} = 0.50$	Perry and Green (1984)
$\lambda_m = 1.66 \times 10^{-4}$	Baillagou and Soong (1985c)
$\lambda_p = 2.5 \times 10^{-4}$	Brandrup et al. (1999)
$\lambda_s = 1.56 \times 10^{-4}$	Perry and Green (1984)
$k_h = 0.43$	Brandrup et al. (1999)

Table 7
Pilot-plant reactor design parameters

Reactor parameter	Unit
$L_1 = 2.160$	m
$L_2 = 0.389$	m
$L_3 = 2.804$	m
$L_4 = 0.440$	m
$d_t = 0.038$	m
$\varepsilon_{\text{mix}} = 0.64$	—
$\alpha_t = 1.7 \times 10^{-4}$	m^2/s
$L_e = 0.034$	m
$\tau_j = 78$	s
$U = U_0 + 0.1\phi_p + 1.2\phi_p^2 - 2.0\phi_p^3$	kJ/s m^2 K

be summarised as

Boundary conditions:

$$\begin{cases} v_z(C_{xf} - C_x)|_{z=0} = -D_e \left.\dfrac{\partial C_x}{\partial z}\right|_{z=0}, \\ \left.\dfrac{\partial C_x}{\partial z}\right|_{z=L_i} = 0, \end{cases} \tag{36}$$

$$\begin{cases} v_z(T_f - T)|_{z=0} = -\alpha_t \left.\dfrac{\partial T}{\partial z}\right|_{z=0}, \\ \left.\dfrac{\partial T}{\partial z}\right|_{z=L_i} = 0, \end{cases} \tag{37}$$

$$\begin{cases} v_{z1}|_{z1=0} = 4(1 + r_{ec})F_f/(\pi d_t^2 \varepsilon_{\text{mix}}), & L_1, \\ v_{z2}|_{z2=0} = v_{z1} r_{ec}/(1 + r_{ec})|_{z1=L_1}, & L_2, \\ v_{z3}|_{z3=0} = v_{z1}/(1 + r_{ec})|_{z1=L_1}, & L_3, \\ v_{z4}|_{z4=0} = v_{z3}|_{z3=L_3}, & L_4, \end{cases} \tag{38}$$

Initial conditions:

$$\begin{cases} C_m(z,0) = C_i(z,0) = C_z(z,0) = 0, \\ \xi_0(z,0) = \xi_1(z,0) = \xi_2(z,0) = 0, \\ \mu_0(z,0) = \mu_1(z,0) = \mu_2(z,0) = 0, \\ T(z,0) = T_j(0) = T_{jsp}. \end{cases} \tag{39}$$

Eqs. (36) and (37) describe the closed–closed boundary conditions of mass and energy transport for each tubular section. The initial conditions given in Eq. (39) describe pure solvent in the reactor at the instant of start-up.

3.5. Model solution

The pilot-plant polymerisation reactor model (Eqs. (1)–(39)) is a mixed system of algebraic, ordinary and partial differential equations. The gPROMS modelling environment was used in this work to solve the equation set. This involved the method of lines to discretise the partial differential equations to a set of ordinary differential equations. Discretisation was through a backward finite difference methods, i.e. a uniform grid of 40 discretisation intervals per tubular section. The resulting system of ordinary differential-algebraic equations were then solved by using a standard solver within the gPROMS environment, SRADAU. In attaining reactor parameters through model fitting, the gEST software was employed within the gPROMS environment, which enabled a least-squares method for estimation. Further details on the gPROMS environment are given by Oh and Pantelides (1996).

4. Results and discussion

4.1. Reactor parameter estimation

The initial overall heat transfer coefficient (U_0) and jacket time constant (τ_j) were estimated using cold run #1, #2 and PMMA #4; a least-squares parameter estimation method was used for this purpose. For each estimation of the dynamic tests, 120 points of on-line jacket and reactor temperature measurements were used. The standard deviation of the temperature measurements were assumed to be 0.4°C. The standard deviation of the U_0 and τ_j estimations were calculated as 0.01 kJ/s m^2 K and 1.6 s, respectively. The value of U_0 then enabled the calculation of the effective length, L_e, in Eq. (29). The estimated initial heat transfer coefficient, U_0, was found to be in good agreement with the theoretical prediction of Eq. (29); see comparisons at the end of Table 1. U_0 was also found to be approximately 4 times higher than that of an equivalent empty tube (i.e. when L_e denotes actual reactor length), which supports the claims made from the static mixer manufacturer (Sulzer, 1997). An average jacket time constant (τ_j) was estimated as 78 s for all three heating/cooling sections. Parameters in Eq. (31) for the

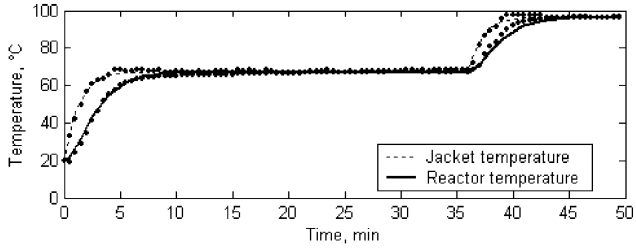

Fig. 3. Reactor and jacket temperature dynamics for cold run #1. (Dots are on-line measurements; lines are model predictions.)

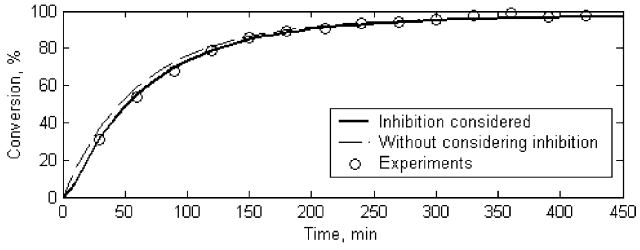

Fig. 4. Batch PMMA experimental verifications of the kinetic model. (80°C, 30% (v/v) monomer, $C_{i0} = 0.0164$ kmol/m^3.)

calculation of U were also attained from the data in run PMMA #4. A total of 21 offline conversion measurements from the 3 sampling points was used for the estimation.

In Fig. 3, measured and calculated temperature response data are shown for the jacket temperature step-change studies with pure xylene. The simple first-order dynamic equation for the jacket is shown to provide an adequate description of the jacket temperature. Likewise, the estimated value of U_0 is shown to give an accurate prediction of the xylene temperature within the reactor.

4.2. Kinetic model verification

The batch PMMA experiments were used to verify the reaction kinetic model, and to quantitatively estimate the effects of inhibition. Fig. 4 shows good correlation between the simulated and experimental conversion profiles, in which all the kinetic parameters are taken from the literature. The presence of inhibitor is shown to cause a slight retardation of the initial polymerisation rate. Such an effect was adequately modelled by the inclusion of inhibitor kinetic constants (k_z and f_z) in the free-radical mechanism. The least-squares parameter estimation method were again used to attain the inhibitor kinetic constants, with the initial values taken from the literature (Brandrup et al., 1999).

4.3. Pilot-scale polymerisation

In experiment PMMA #3, relatively low monomer and high initiator concentrations were used. The simulated and experimental conversion profiles are shown in Fig. 5, in

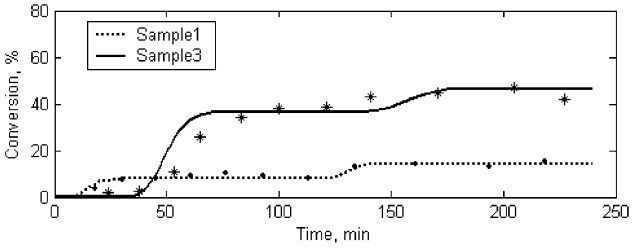

Fig. 5. Comparisons of measured and model predictions of conversions for run PMMA #3. Jacket temperature setpoints changed from 70°C to 80°C after 2 h of reaction. (● experimental sampling 1, ∗ experimental sampling 3.)

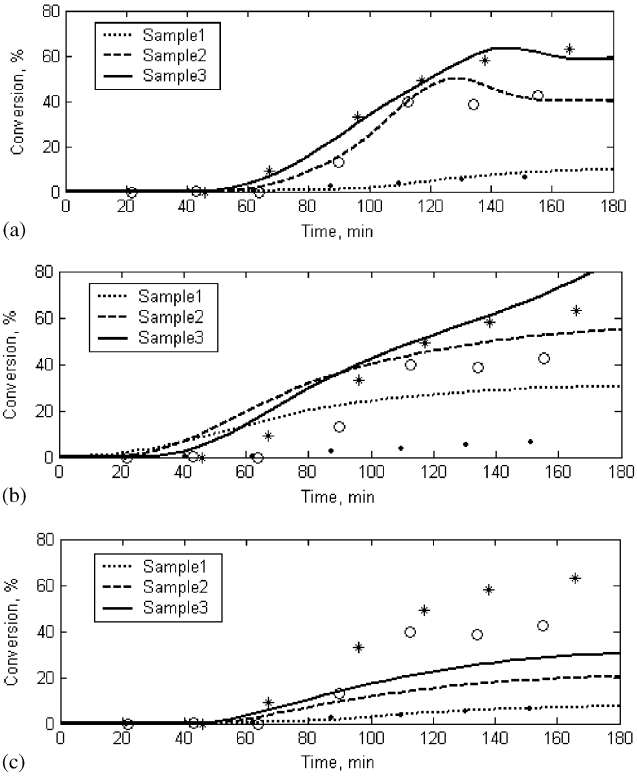

Fig. 6. Comparisons of measured and different model predictions of conversions for run PMMA #4: (a) the full reactor model, (b) model without considering inhibition, (c) isothermal simplification model. (● experimental sampling 1, o experimental sampling 2, ∗ experimental sampling 3.)

which accurate conversion predictions under different temperatures are shown. In experiment PMMA #4, measurements and calculations are shown for the case of a relatively high monomer to solvent ratio, and a low initiator concentration. In this case, there is a much longer induction period, which suggests that the inhibitor has a more significant influence on polymerisation. This is supported by simulations in which the removal of inhibitor kinetics leads to poor predictions of the measured trends; cf. Figs. 6a and b. The full model can accurately predict the dynamic conversion profiles at different sampling points along the tubular reactor.

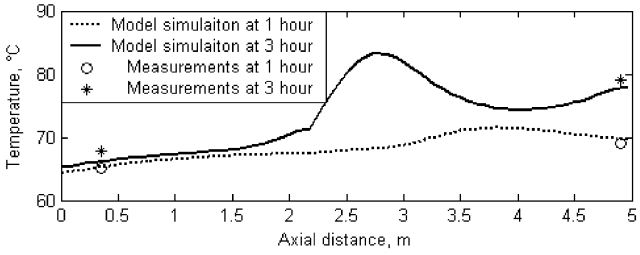

Fig. 7. Model simulations and on-line measurements of temperature profiles along the tubular reactor for run PMMA #4. (Jacket temperature 70°C, reactants feed temperature 20°C.)

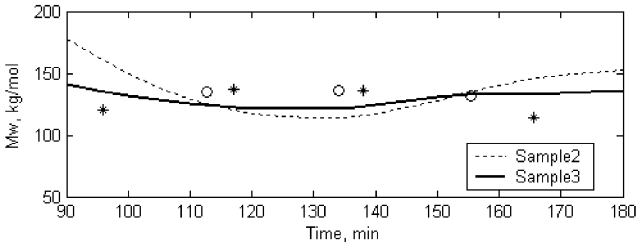

Fig. 8. Model predictions of average molecular weight for run PMMA #4. (o experimental sampling point 2, ∗ experimental sampling point 3.)

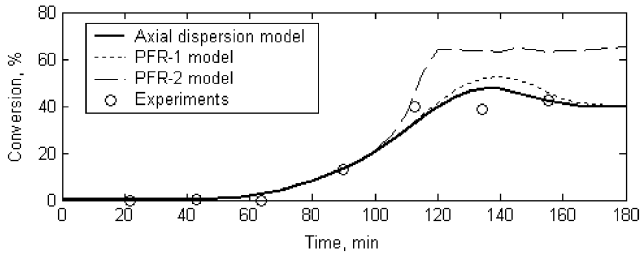

Fig. 9. Comparison of the full axial dispersion model with two simplified ideal plug-flow model predictions of monomer conversion for run PMMA #4.

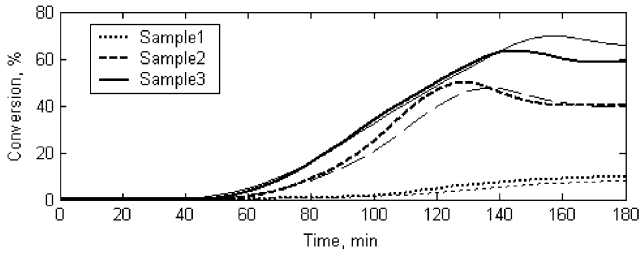

Fig. 10. Comparison of models with constant (thin lines) and variable (thick lines) initiator efficiency f.

The slight overshoot in the predicted and (to a smaller extent) the measured conversion profiles may be due to the transitory effect of inhibition (Vega, Lima, & Pinto, 1997), and possibly the transitory temperature dynamics of the reactor (e.g. propagation of a thermal wave; cf. Fig. 7).

Although SMXL static mixers greatly improve the heat transfer ability of the pilot plant reactor, there is still a high temperature difference between the jacket and reactants, i.e. in the region of 15°C. As shown in Fig. 6c, if isothermal operation is assumed, the polymerisation is predicted to reach much lower final conversions.

Compared with run PMMA #3, run PMMA #4 used a more concentrated monomer solution. At higher conversions, difficulty was met when extracting samples from sampling point 3, due to the high viscosity of the reaction mixture. At the end of the devolatilisation section, solid PMMA was recovered.

The simulated temperature profiles along the tubular reactor are shown in Fig. 7, together with on-line measurements. The temperature at the end of the tube L_3 was estimated using the on-line jacket and reaction temperature measurements, from the devolatilisation section. With the reactor approaching its steady state, the hot spot moved from the back to the middle section. The first temperature measurements at 0.35 m downstream (from the inlet) registered a temperature rise of 3°C, while the end of the reactor registered a temperature rise of 10°C. The maximum temperature difference between cooling jacket and reactants was around 15°C.

Fig. 8 shows the simulated and experimental weight average molecular weight of samples from run PMMA #4. As the conversion increases, the weight average molecular weight decreases from 150 to 114 kg/mol, with the polydispersity index remaining relatively constant at around 1.8, slightly lower than model predictions of about 2.1.

Fig. 9 compares the experimental data from PMMA #4 with two versions of the ideal plug-flow model, and the full axial dispersion model described above. The PFR-1 model assumes a perfect plug flow of reaction species, but in which there is still axial thermal dispersion within the energy balance. The PFR-2 model assumes a perfect plug flow of both mass and energy. It can be seen that the influence of static mixers leads to the near-ideal plug flow of mass, but with an enhancement in thermal dispersion along the reactor length. A possible explanation for this is the additional heat flux arising from the axial thermal conductivity through the static mixers. However, it is interesting to note that deviations from ideal plug flow may in fact be beneficial towards the scaleup of loop mode operation (Nauman, 2001).

Fig. 10 compares the simulated conversion profiles for the case where initiator efficiency is either kept constant ($f \equiv 0.53$) or as a function of free-volume (Eq. (10)). The introduction of a non-constant initiator efficiency appears to only slightly improve the model predictions, and thus seems to introduce unnecessary complexity and uncertain parameters (Eqs. (10)–(12)). Consequently, the assumption of a constant initiator efficiency during the course of the polymerisation is considered appropriate for this particular case.

5. Conclusions

A theoretical model has been developed for the dynamic simulation of polymerisation of a pilot-scale reactor containing in-line static mixers within jacketed tubular sections. Independent experiments were used to establish the temperature dynamics of the reactor, and the validity of the kinetic model in the presence of inhibitor. For a feed monomer concentration of 72% (v/v), and conversions up to 95%, accurate predictions of MMA polymerisation were attained using a non-isothermal and non-adiabatic axially dispersed plug-flow model of the reactor, in which the overall heat transfer coefficient was treated as a distributed parameter. Comparison of the model with an ideal plug-flow simulation indicated that the near-ideal plug flow of mass is approached in the presence of the static mixers. The static mixers were also shown to significantly enhance the tube-side heat transfer characteristics of the reactor, and thus lead to improved temperature control. The model thus provides a good basis for future studies in reactor control, as well as studies under semi-batch operation when the reactor is configured in loop mode.

Notation

c	polymer concentration in the viscosity equation, kg/dm^3
C	parameter in the initiator efficiency equation, dm^3
C_i	initiator concentration, kmol/m^3
C_{if}	inflow initiator concentration, kmol/m^3
C_m	monomer concentration, kmol/m^3
C_{mf}	inflow monomer concentration, kmol/m^3
C_p	heat capacity of reaction mixture, kJ/kg K
$C_{p,m}$	heat capacity of monomer, kJ/kg K
$C_{p,p}$	heat capacity of polymer, kJ/kg K
$C_{p,r}$	heat capacity of steel, kJ/kg K
$C_{p,s}$	heat capacity of solvent, kJ/kg K
C_x	concentration for different species in mass balance equation, kmol/m^3
C_{xf}	inflow concentration for tubular section $L_{1–4}$, kmol/m^3
C_z	inhibitor concentration, kmol/m^3
C_{zf}	inflow inhibitor concentration, kmol/m^3
D	parameter in the gel effect constitutive equation, dimensionless
D_e	axial mass dispersion coefficient, m^2/s
D_l	molecular diffusion coefficient, m^2/s
d_t	outer diameter of reactor tube, m
f	initiator efficiency, dimensionless
f_0	initial initiator efficiency, dimensionless
F_f	total inflow rate of reactants, m^3/s
F_r	recycle flow rate, m^3/s
f_z	number of radicals consumed per inhibitor molecule, dimensionless
h_i	tube side heat transfer coefficient, kJ/s m^2 K
$-\Delta H_P$	heat of polymerisation, kJ/kmol
k_d	kinetic constant for initiator decomposition, 1/s
k_{fm}	kinetic constant for transfer to monomer, m^3/kmol s
k_{fs}	kinetic constant for transfer to solvent, m^3/kmol s
k_h	Huggins constant, dimensionless
k_i	kinetic constant for primary radical formation, m^3/kmol s
k_p	kinetic constant for propagation of free radical, m^3/kmol s
k_{p0}	initial kinetic constant for propagation of free radical, m^3/kmol s
k_t	kinetic constant for termination, m^3/kmol s
k_{t0}	initial kinetic constant for termination, m^3/kmol s
k_{tc}	kinetic constant for termination by combination, m^3/kmol s
k_{td}	kinetic constant for termination by disproportionation, m^3/kmol s
k_z	kinetic constant for inhibition, m^3/kmol s
k_{θ_p}	parameter in the gel effect constitutive equation, 1/s
k_{θ_t}	parameter in the gel effect constitutive equation, 1/s
$L_{1–4}$	tubular length of the reactor sections, m
M_n	number average molecular weight of the polymer, kg/kmol
M_w	weight average molecular weight of the polymer, kg/kmol
MW_i	molecular weight of initiator, kg/kmol
MW_m	molecular weight of monomer, kg/kmol
MW_s	molecular weight of solvent, kg/kmol
N_{Bo}	Bodenstein number, dimensionless
N_{Gz}	Graetz number, dimensionless
N_{Pr}	Prandtl number, dimensionless
N_{Re}	Reynolds number, dimensionless
PDI	polydispersity index, dimensionless
R	universal gas constant, kJ/kmol K
r_{ec}	recycle ratio of the loop section, dimensionless
R_x	reaction rate of different species, kmol/m^3 s
T	temperature, K
T_f	inflow temperature of reactants, K
T_j	jacket temperature, K
T_{jsp}	jacket temperature setpoint, K
U	overall heat transfer coefficient, kJ/s m^2 K
U_0	initial overall heat transfer coefficient, kJ/s m^2 K
V_F	free volume, dm^3
$V_{F\mathrm{cr}}$	critical free volume, dm^3
v_z	axial velocity, m/s
X_m	monomer conversion, dimensionless

Greek letters

$\alpha_1, \alpha_2, \alpha_3$	parameters in the overall heat transfer coefficient equation, kJ/s m^2 K
α_t	axial thermal dispersion coefficient, m^2/s

ε_{mix}	void fraction of reactor, dimensionless
ε_r	constant for static mixer and reactor wall, dimensionless
ϕ_m	volume fraction of monomer, dimensionless
ϕ_p	volume fraction of polymer, dimensionless
ϕ_s	volume fraction of solvent, dimensionless
η	viscosity, Pa s
$[\eta]$	intrinsic viscosity, dm^3/kg
η_0	solvent (monomer) viscosity, Pa s
η_{sp}	specific viscosity, dimensionless
η_w	viscosity at the reactor wall, Pa s
λ_m	thermal conductivity of monomer, kJ/s m K
λ_{mix}	thermal conductivity of reaction mixture, kJ/s m K
λ_p	thermal conductivity of polymer, kJ/s m K
λ_s	thermal conductivity of solvent, kJ/s m K
μ_i	ith moment of "dead" polymer chains, $kmol/m^3$
ρ_i	density of initiator, kg/m^3
ρ_m	density of monomer, kg/m^3
ρ_{mix}	density of reaction mixture, kg/m^3
ρ_p	density of polymer, kg/m^3
ρ_r	density of steel, kg/m^3
ρ_s	density of solvent, kg/m^3
τ_j	time constant of jacket dynamics, s
ξ_i	ith moment of "living" polymer chains, $kmol/m^3$

Subscripts

0	initial value
f	feed
i	initiator
j	jacket
m	monomer
p	polymer
s	solvent
x	symbol for different species
z	inhibitor, axial

Acknowledgements

The authors would like to thank Professor Dame J.S. Higgins, Professor C. C. Pantelides and Dr. S. Asprey from Imperial College for their advice and helpful discussions. Special thanks to Mr. M. Sadler for the many modifications on the supplied pilot-plant reactor, and help in carrying out the experiments, and to Carolina Galmes for her help with the GPC studies. The authors would also like to thank the EPSRC for the funding of this work particularly in the set-up of the interdisciplinary research group in Polymers, Properties and Polymerisation Processes (P4).

References

Baillagou, P. E., & Soong, D. S. (1985a). Major factors contributing to the nonlinear kinetics of free-radical polymerization. *Chemical Engineering Science*, *40*, 75–86.

Baillagou, P. E., & Soong, D. S. (1985b). Molecular weight distribution of products of free radical nonisothermal polymerization with gel effect. Simulation for polymerization of poly(methyl methacrylate). *Chemical Engineering Science*, *40*, 87–104.

Baillagou, P. E., & Soong, D. S. (1985c). Free-radical polymerization of methyl methacrylate in tubular reactors. *Polymer Engineering and Science*, *25*, 212–231.

Brandrup, J., Immergut, E. H., & Grulke, E. A. (1999). *Polymer Handbook* (4th ed.). New York: Wiley.

Chen, C. C., & Nauman, E. B. (1989). Verification of a complex, variable viscosity model for a tubular polymerization reactor. *Chemical Engineering Science*, *44*, 179–188.

Dube, M. A., Soares, J. B. P., Penlidis, A., & Hamielec, A. E. (1997). Mathematical modeling of multicomponent chain-growth polymerizations in batch, semibatch, and continuous reactors: a review. *Industrial and Engineering Chemistry Research*, *36*, 966–1015.

Fleury, P. A., Meyer, Th., & Renken, A. (1992). Solution polymerization of methyl-methacrylate at high conversion in a recycle tubular reactor. *Chemical Engineering Science*, *47*, 2597–2602.

Ghosh, P., Gupta, S. K., & Saraf, D. N. (1998). An experimental study on bulk and solution polymerization of methyl methacrylate with responses to step changes in temperature. *Chemical Engineering Journal*, *70*, 25–35.

Hamer, J. W., & Ray, W. H. (1986a). Continuous tubular polymerization reactors—I. A detailed model. *Chemical Engineering Science*, *41*, 3083–3093.

Hamer, J. W., & Ray, W. H. (1986b). Continuous tubular polymerization reactors—II. Experimental studies of Vinyl Acetate polymerization. *Chemical Engineering Science*, *41*, 3095–3100.

Melo, P. A., Biscaia Jr., E. C., & Pinto, J. C. (2001a). Thermal effects in loop polymerization reactors. *Chemical Engineering Science*, *56*, 6793–6800.

Melo, P. A., Pinto, J. C., & Biscaia Jr., E. C. (2001b). Characterization of the residence time distribution in loop reactors. *Chemical Engineering Science*, *56*, 2703–2713.

Nauman, E. B. (1994). Polymerization reactor design. In C. McGreavy (Ed.), *Polymer reactor engineering* (p. 137). New York: VCH.

Nauman, E. B. (2001). *Chemical reactor design, optimization and scaleup*. New York: McGraw-Hill.

Oh, M., & Pantelides, C. C. (1996). A modelling and simulation language for combined lumped and distributed parameter systems. *Computers and Chemical Engineering*, *20*, 611–633.

Perry, R. H., & Green, D. (1984). *Perry's chemical engineers' handbook* (6th ed.). New York: McGraw-Hill.

Pinto, J. C., & Ray, W. H. (1995). The dynamic behaviour of continuous solution polymerization reactors—VII. Experimental study of a copolymerisation reactor. *Chemical Engineering Science*, *50*, 715–736.

Pinto, J. C., & Ray, W. H. (1996). The dynamic behaviour of continuous solution polymerization reactors—IX. Effects of inhibition. *Chemical Engineering Science*, *51*, 63–79.

Soroush, M., & Kravaris, C. (1992). Nonlinear control of a batch polymerization reactor: an experimental study. *A.I.Ch.E. Journal*, *38*, 1429–1448.

Sulzer. (1997). *Mixing and reaction technology*. Sulzer Chemtech Ltd, Winterthur, Switzerland, No.23.27.06.40-VI.97–100.

Tefera, N., Weickert, G., & Westerterp, K. R. (1997). Modeling of free radical polymerization up to high conversion. II. Development of a mathematical model. *Journal of Applied Polymer Science*, *63*, 1663–1680.

Vega, M. P., Lima, E. L., & Pinto, J. C. (1997). Modeling and control of tubular solution polymerization reactors. *Computers and Chemical Engineering*, *21*(Suppl.), S1049–S1054.

Zacca, J. J., & Ray, W. H. (1993). Modelling of the liquid phase polymerization of olefins in loop reactors. *Chemical Engineering Science*, *48*, 3743–3765.